Check for updates

View Article Online
View Journal

Journal of
Materials Chemistry C

Materials for optical, magnetic and electronic devices

Accepted Manuscript

This article can be cited before page numbers have been issued, to do this please use: X. Zhang, L. Einhaus, A. Huijser and J. E. ten Elshof, *J. Mater. Chem. C*, 2024, DOI: 10.1039/D4TC02231A.

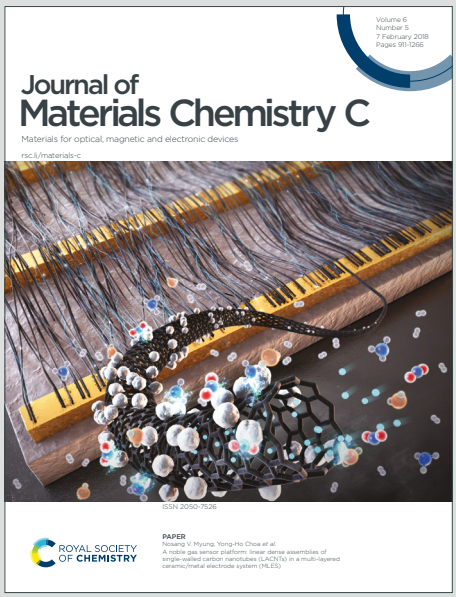

This is an Accepted Manuscript, which has been through the Royal Society of Chemistry peer review process and has been accepted for publication.

Accepted Manuscripts are published online shortly after acceptance, before technical editing, formatting and proof reading. Using this free service, authors can make their results available to the community, in citable form, before we publish the edited article. We will replace this Accepted Manuscript with the edited and formatted Advance Article as soon as it is available.

You can find more information about Accepted Manuscripts in the Information for Authors.

Please note that technical editing may introduce minor changes to the text and/or graphics, which may alter content. The journal's standard Terms & Conditions and the Ethical guidelines still apply. In no event shall the Royal Society of Chemistry be held responsible for any errors or omissions in this Accepted Manuscript or any consequences arising from the use of any information it contains.

ROYAL SOCIETY OF CHEMISTRY

rsc.li/materials-c

View Article Online
DOI: 10.1039/D4TC02231A

Phase Distribution Regulation of Formamidinium-based Quasi-2D Perovskites through Solution Engineering

Xiao Zhang[1], Lisanne Einhaus[2], Annemarie Huijser[2], Johan E. ten Elshof[1]

[1] Inorganic Materials Science Group, MESA+ Research Institute, University of Twente, 7500 AE Enschede, the Netherlands

[2] PhotoCatalytic Synthesis Group, MESA+ Research Institute, University of Twente, 7500 AE Enschede, the Netherlands

Open Access Article. Published on 22 2024. Downloaded on 22-08-2024 8:22:30.
This article is licensed under a Creative Commons Attribution 3.0 Unported Licence.

Abstract

Quasi-2D perovskites have attracted attention as potential solar energy absorber materials due to their balanced efficiency and stability, and their unique quantum-well structures. In order to facilitate directional exciton and charge carrier transport and preferential energy transfer landscape in photovoltaic thin films, the phase distribution formed by the different types of microstructural domains should be regulated. In this work, the Dion-Jacobson-type spacer 1,4-phenylenedimethanammonium (PDMA) was used, and different strategies were pursued to control the phase distribution in formamidinium-based (FA) quasi-2D perovskites based on the composition of (PDMA)$FA_4Pb_5I_{16}$. In general, doping with FACl modulated the crystallization kinetics, forming 2D low-*n* crystals on the top surface or a reversed-gradient phase distribution, depending on whether excess or substitutional doping was employed. Alternatively, mixing with a Ruddlesden-Popper spacer helped bridging to adjacent octahedra in pure PDMA-based perovskites and improve crystallization, while regulating the quantum-well structures into a normal-gradient phase distribution, where 2D domains resided on the bottom side. By combining FACl doping and spacer mixing, the film showed both a reversed-gradient phase distribution and larger vertically aligned grains. This work contributes to the knowledge how to manipulate and regulate the phase distribution in FA-based quasi-2D perovskites, and further paves the way for fabricating corresponding devices with high efficiency and stability.

Keywords

Quasi-2D perovskite, formamidinium, phase distribution, solution engineering, additive doping, spacer mixing

Journal of Materials Chemistry C Accepted Manuscript

View Article Online
DOI: 10.1039/D4TC02231A

Open Access Article. Published on 22 2024. Downloaded on 22-08-2024 8:22:30.
This article is licensed under a Creative Commons Attribution 3.0 Unported Licence.

Journal of Materials Chemistry C Accepted Manuscript

1. Introduction

Metal halide perovskite (MHP) is currently one of the most popular solar energy absorber materials to boost photovoltaic performance. Among the different types of MHPs, two-dimensional (2D) perovskites have attracted intensive attention in more recent years, since they comprise hydrophobic organic spacers which provide higher long-term stability against external stimuli under operational conditions, such as moisture, heat, oxygen and ion migration, compared to their 3D analogues.[1-11] Although the power conversion efficiency (PCE) of 2D perovskites is still lagging behind that of the 3D perovskites, the record PCE of formamidinium (FA)-based 2D perovskite solar cells (PSC) has reached over 20%, achieving a balanced efficiency and intrinsic stability.[12]

As depicted in **Figure 1**, by introducing large organic spacers along the (100) plane of 3D perovskites[13-15], 2D and quasi-2D perovskites with a chemical formula of $(L)_m(A)_{n-1}(B)_n(X)_{3n+1}$ are formed, where L represents the large organic spacers, A are small monovalent cations (e.g., methyl ammonium MA^+, FA^+, Cs^+) fitting in the $[BX_6]^{4-}$ octahedral frameworks, B are divalent cations (e.g., Pb^{2+}, Sn^{2+}), X are halide ions (e.g., I^-, Br^-, Cl^-), *m* depends on the spacer types (*m* = 2 for a monovalent Ruddlesden-Popper spacer, *m* = 1 for a divalent Dion-Jacobson spacer), and *n* represents the average number of inorganic layers between two organic spacers (*n* = 1 for pure 2D perovskites, $n \geq 2$ for quasi-2D perovskites, $n = \infty$ for 3D perovskites).[16-21] Since the value of *n* can vary locally on microscale, we employ the term <*n*> further on to denote the global average value in this paper.

In our work, the Dion-Jacobson (DJ) spacer 1,4-phenylenedimethanammonium (PDMA) was primary used as L-site spacer. Other Ruddlesden-Popper (RP) spacers, such as propylammonium (PA), *n*-butylammonium (BA), allylammonium (ALA), phenylmethylammonium (PMA), and phenethylammonium (PEA), were also used for comparison or for mixing with PDMA. FA was used as A-site cation, since FA-based perovskites have a higher thermal stability than the methylammonium (MA) series, owing to the higher sublimation temperature of FA compared with MA.[22] Moreover, FA-based perovskites have a smaller bandgap than the MA series because of the increasing Pb-I-Pb angles induced by the larger size of FA, thus covering a larger part of the solar spectrum.[23-26] Therefore, FA-based perovskites have a higher potential to generate solar cells with both high efficiency and high thermal stability. However, due to the large size of FA, the Goldschmidt tolerance factor of the $FAPbI_3$ perovskite structure approaches its maximum value 1, beyond which the cubic phase with corner-shared octahedra is not structurally stable.[27, 28] In fact, $FAPbI_3$ has multiple polymorphic phases, of which the photo-inactive hexagonal δ-phase, or yellow phase, is the stable phase at room temperature. The phase transition into the desired cubic α-phase, or black phase takes place at higher temperature (150-185 °C).[29, 30] The use of N-methyl-2-pyrrolidone (NMP) as co-solvent together with the primary solvent dimethyl formamide (DMF) can yield a stable α-phase $FAPbI_3$. NMP has a weak intermolecular interaction with DMF but strongly coordinates with PbI_2 and FAI. The as-formed PbI_2-NMP intermediate phase can directly convert into the α-phase after annealing.[31]

Additive doping is another effective way to form α-phase $FAPbI_3$. Chloride salt derivatives (e.g. MACl, FACl, $PbCl_2$) can suppress the formation of δ-phase and support the formation of α-phase, regulating the crystal growth orientation.[32-34] By incorporating N,N-dimethylimidodicarbonimidic diamide hydroiodide (DIAI), the intermediate phase FAI-PbI_2-dimethyl sulfoxide (DMSO) complex is eliminated, so that the δ-phase is directly converted into the desired phase α-$FAPbI_3$.[35] Bu et al. used both the co-solvent system DMF/NMP and MACl as additive to grow high-quality α-phase FA-based 3D perovskite

View Article Online
DOI: 10.1039/D4TC02231A

solar cells with a PCE of 24.02%.[36] However, a comprehensive understanding of what controls the crystallization, and especially the phase distribution in quasi-2D perovskites, is still lacking.

For quasi-2D perovskite thin films fabricated with the solution method with a certain <*n*> value, there are typically multiple local microstructural domains of different *n* values coexisting, where low-*n* domains (*n* = 1, 2) and high-*n* domains (*n* = 4, 5 …) are heterogeneously distributed or concentrated in different areas within the film. The multiple quantum-well structures form a so-called phase distribution, which determines the charge carrier transport pathways and energy transfer landscape.[37-43] Different phase distributions (e.g. normal-gradient with low-*n* domains at the bottom and high-*n* domains at the top of the film, or reversed-gradient with reversed distribution of low-*n* and high-*n* domains) are suitable for different solar cell configurations (e.g. p-i-n where the hole transport layer is at the bottom interface and the electron transport layer at the top interface, or n-i-p configuration) due to different energy level alignments. Therefore, knowing how to tune the phase distribution of quasi-2D perovskites is of vital importance.

Our work aims at fabricating stable α-phase FA-based quasi-2D perovskites with controlled phase distribution. Through FACl doping, both by excess and substitutional doping, the phase distribution can be regulated into a reversed-gradient manner, enabling to steer the directionality of exciton and charge transport, and protecting the film from moisture penetration. Spacer engineering was also carried out by mixing Dion-Jacobson spacer PDMA and two Ruddlesden-Popper spacers, ALA and PA. The phase distribution of *n*-domains can be further regulated into either a similar reversed-gradient or a normal-gradient manner, facilitating an energy transfer cascade, favouring directional exciton and charge transport and a potential electron tunnelling through the interlayer [44], thus paving the way towards future devices with high efficiency and stability.

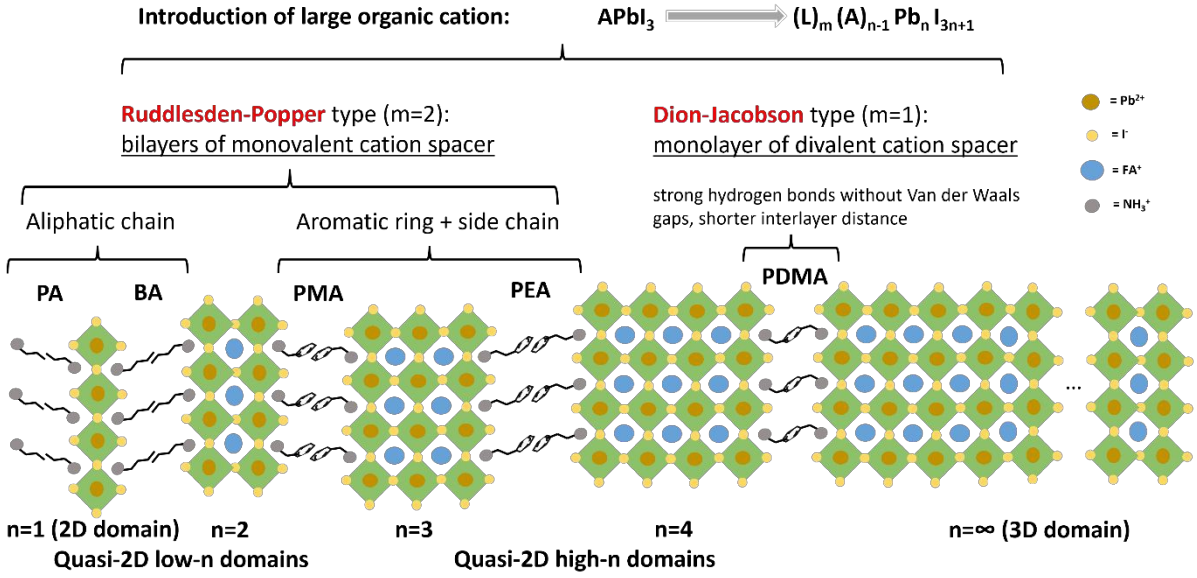

Figure 1. Schematic illustration of the structure and phase distribution of quasi-2D perovskites with Ruddlesden-Popper-type and Dion-Jacobson-type spacers.

Open Access Article. Published on 22 2024. Downloaded on 22-08-2024 8:22:30.
This article is licensed under a Creative Commons Attribution 3.0 Unported Licence.

Journal of Materials Chemistry C Accepted Manuscript

View Article Online
DOI: 10.1039/D4TC02231A

Open Access Article. Published on 22 2024. Downloaded on 22-08-2024 8:22:30.
This article is licensed under a Creative Commons Attribution 3.0 Unported Licence.

Journal of Materials Chemistry C Accepted Manuscript

2. Results and Discussion

2.1 Fabrication of stable α-phase quasi-2D perovskites $(PDMA)(FA)_4Pb_5I_{16}$

Following the same fabrication conditions as with the MA series in our previous work [45], i.e. using a 10:1 volume ratio of DMF:DMSO as the solvent mixture, using the hot-casting processing method and post-annealing at 100 °C, the quasi-2D perovskite $(PDMA)(FA)_4Pb_5I_{16}$ showed the photo-inactive yellow phase or δ-phase (**Figure 2a**), which is the stable phase at room temperature for $FAPbI_3$. The phase transition into a corner-shared cubic phase can only occur by providing more thermal energy. Therefore, we increased the post-annealing temperature to 150 °C. Since hot-casting method by pre-heating the substrate only changed the reaction kinetics, but not the intermediates chemistry, we changed the processing to the anti-solvent method, by dripping chlorobenzene (CB) onto the as spin-coated perovskite precursor solution, to induce a fast supersaturation state and solvent extraction. Then, we conducted an orthogonal experiment to investigate which solvent combination and additive ratio could produce a stable black phase or α-phase. For the solvent mixture, we selected 4:1 (v/v) DMF:DMSO and 9:1 (v/v) DMF:NMP, while for additive doping, we selected MACl and ammonium thiocyanate (NH_4SCN) in different molar ratios with respect to constant Pb^{2+} concentration, or a mixture of the two (**Table S1**). The results shown in **Figure 2a** and **Figure S1**, with 9:1 (v/v) DMF:NMP as the solvent combination and 10 mol% of excess MACl addition indicated a clean α-phase without other phase impurities, prevailing other solvent combinations and additive doping ratios.

In order to verify the universal feasibility of the new fabrication condition, other Ruddlesden-Popper spacers (PA, BA, PMA, PEA) were also employed. As shown in the X-ray diffractograms in **Figure S2a**, the fabricated quasi-2D perovskite films with $\langle n \rangle$ = 5 all showed the α-phase without δ-phase. The appearance of a small fraction of PbI_2 in $(PEA)(FA)_4Pb_5I_{16}$ may have been caused by annealing-induced thermal degradation. The bandgaps of the quasi-2D perovskites were in the range of 1.53-1.54 eV (see Tauc plot in **Figure S2b**), smaller than in the MA series (1.60-1.63 eV), which illustrates the advantage over the MA series in absorbing a larger part of the solar spectrum. Therefore, it can be concluded that the synergistic strategies of solvent engineering, additive doping and processing methods successfully fabricated the stable α-phase of FA-based quasi-2D perovskites with multiple L-site spacers.

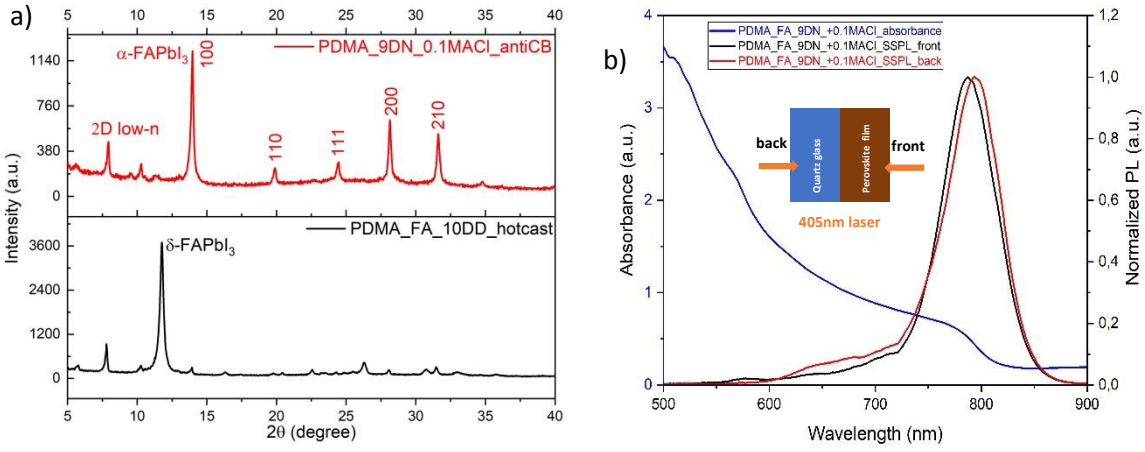

Figure 2. Crystallography and phase distribution of quasi-2D perovskites $(PDMA)(FA)_4Pb_5I_{16}$. (a) Powder X-ray diffractograms of δ-phase and α-phase perovskites made from different precursor solution inks and processing methods. (b) UV-Vis absorption spectra and steady-state

View Article Online
DOI: 10.1039/D4TC02231A

photoluminescence from both front (perovskite) and back (substrate) sides of the quasi-2D perovskite thin film with <*n*> = 5. The inset shows the illumination directions.

Figure 2b shows the UV-Vis absorption and steady-state photoluminescence (PL) spectra. The latter were recorded using both front and back excitation with a 405 nm laser source. Considering that the local 2D low-*n* domains (between 530 and 730 nm) existed at both the top and the bottom sides of the film, it implies that the phase distribution in quasi-2D perovskites $(PDMA)(FA)_4Pb_5I_{16}$ was not fully regulated. Different model systems were built to describe the phase distribution in the quasi-2D perovskites. From a molecular-scale (local) perspective, 2D domains with different *n* values are interspersed in the 3D domain matrix with a concentration variation in different areas of the film. This may also explain why the PL bands of the 3D domains were observed by both front side and back side excitation. In contrast, in a continuum model the 3D domain reside mainly on one side, and the 2D low-*n* domains lie mostly on the other side, thus forming a phase gradient in the film thickness direction. Both model systems with regulated phase distributions can induce a sequential energy transfer cascade and boost the photo-induced charge carrier separation and extraction.[46] But irregular phase distributions, as in the case of the $(PDMA)(FA)_4Pb_5I_{16}$ film in **Figure 2b**, implies that microstructural domains with different quantum-well structures are randomly distributed in the film, which may lead to blocked and impeded charge transport paths, and accelerated charge carrier recombination. Therefore, the phase distribution of FA-based quasi-2D perovskites needs further regulation through manipulating the precursor solution and processing methods.

Open Access Article. Published on 22 2024. Downloaded on 22-08-2024 8:22:30.
This article is licensed under a Creative Commons Attribution 3.0 Unported Licence.

Journal of Materials Chemistry C Accepted Manuscript

View Article Online
DOI: 10.1039/D4TC02231A

2.2 Manipulation strategies for phase distribution regulation

2.2.1 Additive doping with excess FACl

First, we attempted tuning of the additive to manipulate the phase distribution of quasi-2D perovskite (PDMA)$(FA)_4Pb_5I_{16}$. Although MA in MACl additive has a low sublimation temperature and is mostly removed after annealing, it can also remain in the film and become involved in A-site cation mixing, shifting the optical bandgap. Therefore, the additive was changed from MACl to FACl, in order to eliminate the impact of the residual MA in the film, and maintain the phase purity.

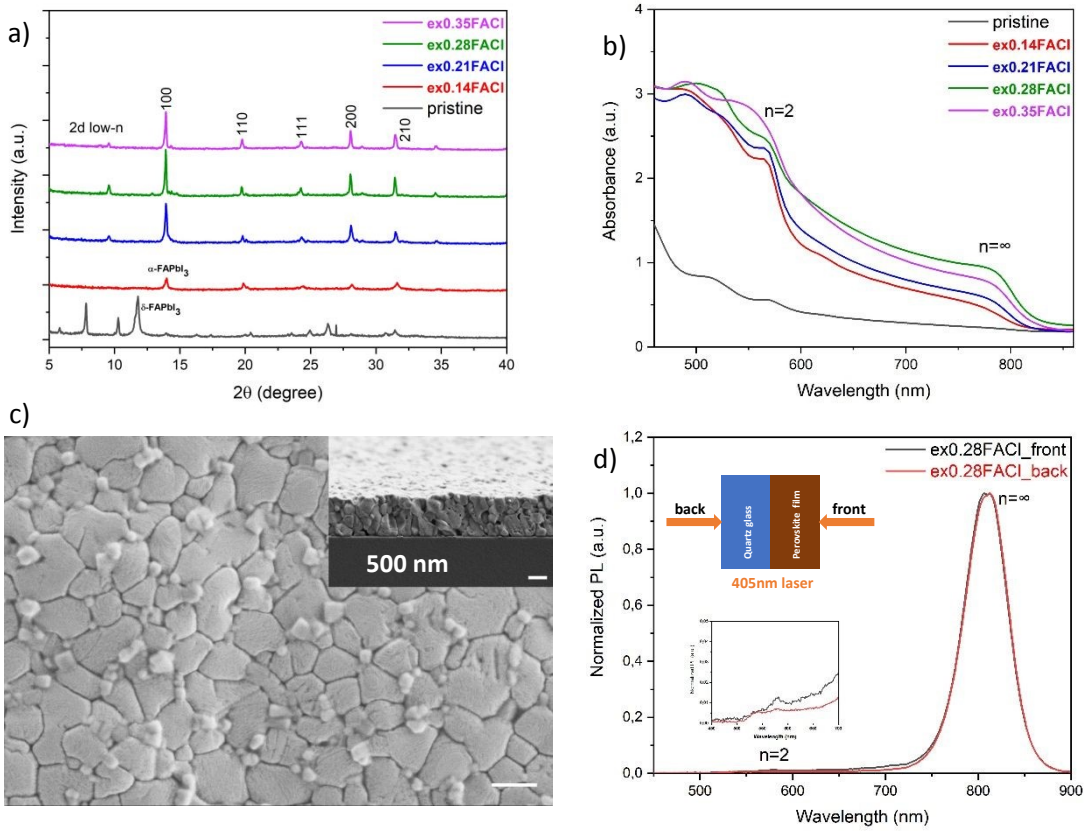

Figure 3. Crystallography, optical properties, surface morphology and phase distribution of quasi-2D perovskites (PDMA)$(FA)_4Pb_5I_{16}$ with 14-35 mol% excess FACl doping. (a) Powder X-ray diffractograms. (b) UV-Vis absorption spectra. (c) Surface morphology of the film with 28 mol% excess FACl addition. Inset is the cross-sectional view, both scale bars are 500 nm. (d) Steady-state PL of the film with 28 mol% excess FACl addition, recorded from front (perovskite) and back (substrate) side illuminations at 405 nm. The inset shows the zoomed-in PL signal in the wavelength range between 450 nm and 700 nm.

In principle, doping can be performed in two ways. The first one is to add excess FACl to the precursor solution of the stoichiometric composition of (PDMA)$(FA)_4Pb_5I_{16}$. With increasing excess FACl, the film showed a stable α-phase and increased crystallinity (**Figure 3a**). The degree of light absorption was also enhanced, especially for the film with 28 mol% excess FACl, which had a sharp absorption onset edge representing the 3D domain, and an excitonic band around 580 nm representing the 2D *n* = 2

Open Access Article. Published on 22 2024. Downloaded on 22-08-2024 8:22:30.
This article is licensed under a Creative Commons Attribution 3.0 Unported Licence.

Journal of Materials Chemistry C Accepted Manuscript

View Article Online
DOI: 10.1039/D4TC02231A

domain (**Figure 3b**). From the steady-state PL data in **Figure 3d**, the 3D domain was detected by both front and back excitation, but there was also a weak *n* = 2 PL band from the perovskite side, consistent with the UV-Vis absorption spectra. This likely implies that the 2D *n* = 2 domain grew preferentially on the top surface of the film, while the bulk was 3D domain, hence forming a regulated phase distribution. This result was confirmed by the surface morphology shown in **Figure 3c**, where compared to the pristine quasi-2D film (**Figure S3a**), the grains were larger (average grain size 500 nm) with some crystals on the surface, especially at grain boundaries. A possible reason may be that with increasing FACl additive, the crystallization kinetics are retarded, and the large spacer cations at the bottom of the solution have more time to diffuse towards the top surface upon post-annealing. The crystals of 2D *n* = 2 local domains eventually accumulate at the grain boundaries of the 3D domain, passivating defects and suppressing the non-radiative recombination centers. The proposed mechanism of film growth and regulated phase distribution is schematically illustrated at the end of this section.

Open Access Article. Published on 22 2024. Downloaded on 22-08-2024 8:22:30.
This article is licensed under a Creative Commons Attribution 3.0 Unported Licence.

2.2.2 Substitutional doping with FACl

The other method of doping with the additive is to substitute FAI partially by FACl, and to keep the concentration of FAI+FACl constant, which is called compensated or substitutional doping. Upon replacing 50 mol% of FAI with FACl, both crystallinity and light absorption were slightly enhanced (**Figure 4a and 4b**). An over-dose of 75 mol% of FACl substitution caused the formation of a PbI_2 phase (2θ = 12.8°) and reduced light absorption due to degradation-induced quenching. The crystalline grains were not as large as in the film with 28 mol% excess FACl, but vertical growth alignment was more obvious, as evident from the compact and large grains in the cross-sectional view in **Figure 4c** can be observed, which may facilitate charge transport in the vertical direction. In the steady-state PL in **Figure 4d**, there was only one dominating band for the back excitation representing the 3D domain, while for the front excitation, except for the 3D domain, there were also two small emission bands representing 2D *n* = 1 and *n* = 3 domains. In comparison to the pristine film in **Figure 2b**, the film with 50 mol% substituted FACl additive had a different phase distribution. More specifically, the location of 2D low-*n* domains changed from the bottom side to the top side, embedded in the 3D domain matrix, thus forming a reverse-gradient phase distribution. An illustrated schematic showing film growth and regulated phase distribution is shown at the end of this section. Recently, the concept of using a 2D spacer as a passivation layer on top of 3D perovskites to increase the stability of 3D perovskites has become popular [47-52], but additional post-treatment is usually needed, for instance an extra spin-coating step with 2D spacer ink and an extra annealing step, which might also induce thermal degradation and a non-stoichiometric composition.[53, 54] In contrast, substitutional FACl doping can produce a similar assembled 2D passivation layer without additional post-treatment, making it a facile strategy to protect the film from moisture penetration due to the hydrophobic nature of the large organic spacers that are present. The passivation effect is beyond the scope of this research. Nevertheless, we suggest that a reversed-gradient phase distribution is more suitable for an n-i-p solar cell configuration than for a p-i-n configuration, since the 2D low-*n* domains with higher exciton binding energies can also serve as electron blocker. Therefore, an electron transport layer (ETL) at the bottom interface can extract electrons more efficiently, and a hole transport layer (HTL) at the top interface can do the same for extracting holes. The majority of all quasi-2D perovskites have a normal-

Journal of Materials Chemistry C Accepted Manuscript

View Article Online
DOI: 10.1039/D4TC02231A

gradient phase distribution. Therefore, changing the phase distribution provides an extra handle to improve the photovoltaic performance when considering a whole solar cell architecture.

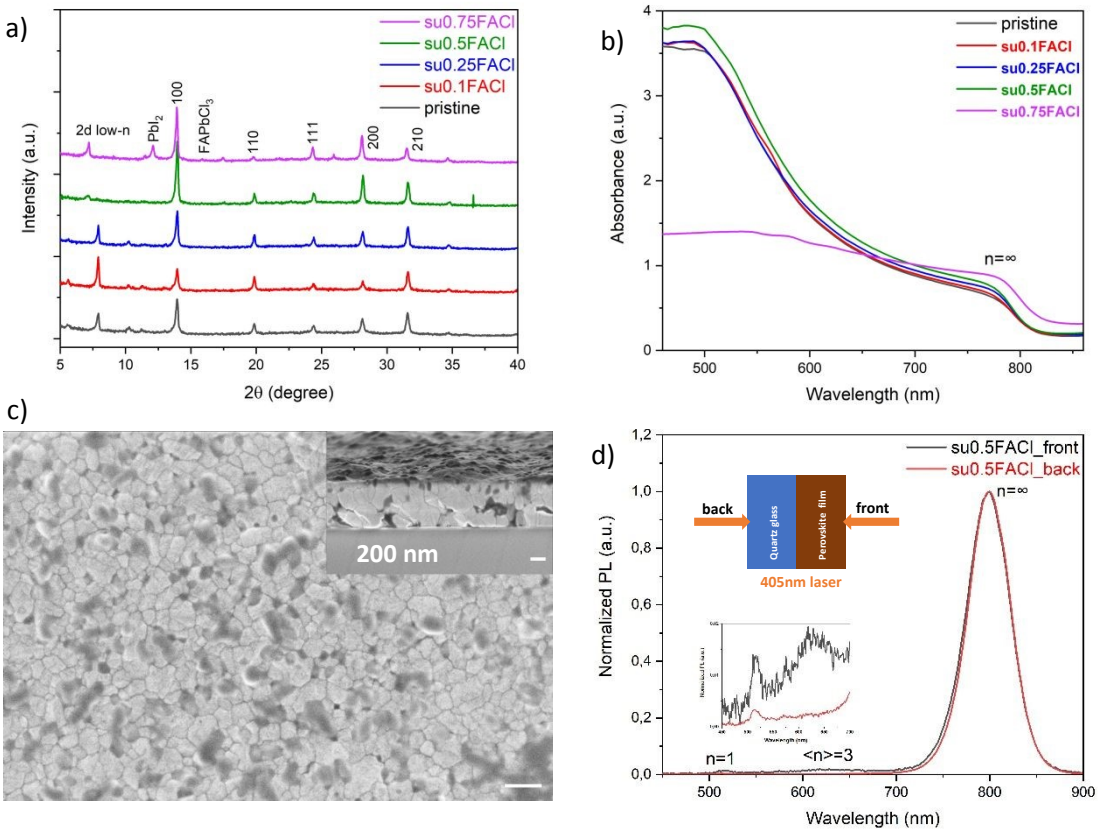

Figure 4. Crystallography, optical properties, surface morphology and phase distribution of quasi-2D perovskites $(PDMA)(FA)_4Pb_5I_{16}$ with compensated FACl additive doping. (a) Powder X-ray diffractograms. (b) UV-Vis absorption spectra. (c) Surface morphology of the film with 50 mol% FACl substitution. Inset is the cross-sectional view, both scale bars are 200 nm. (d) Steady-state PL spectra of the film with 50 mol% FACl substitution for front (perovskite) and back (substrate) side illuminations at 405 nm. The inset shows the zoomed-in PL signal in the wavelength range between 450 nm and 700 nm.

Open Access Article. Published on 22 2024. Downloaded on 22-08-2024 8:22:30.
This article is licensed under a Creative Commons Attribution 3.0 Unported Licence.

Journal of Materials Chemistry C Accepted Manuscript

View Article Online
DOI: 10.1039/D4TC02231A

Open Access Article. Published on 22 2024. Downloaded on 22-08-2024 8:22:30.
This article is licensed under a Creative Commons Attribution 3.0 Unported Licence.

Journal of Materials Chemistry C Accepted Manuscript

2.2.3 Spacer mixing of PDMA and ALA

Following the principles of spacer mixing in our previous work where we found that different types of spacers should have similar interlayer distances between the $[PbI_6]^{4-}$ layers and should have an appropriate steric hindrance effect [45], spacer mixing was also conducted in this work. First, a new Ruddlesden-Popper spacer ALA was used as the co-spacer mixed together with the Dion-Jacobson spacer PDMA. From the XRD data of pure $(ALA)_2PbI_4$, we calculated its interlayer distance, which is 12.95 Å, slightly larger than that of $(PDMA)PbI_4$, which is 12.36 Å (**Figure 5a**). The two spacers can be mixed together, and still maintain the perovskite octahedral frameworks and quantum-well structures .[45] Moreover, the benzyl rings in the PDMA spacer comprises π-conjugated bonds, and the ALA spacer contains C=C double bonds, both of which can form (conjugated) π-bonds, potentially facilitating electron tunnelling through the interlayer [44], mitigating the quantum and dielectric confinement, and having a high potential to increase the charge conductivity.[55-59]

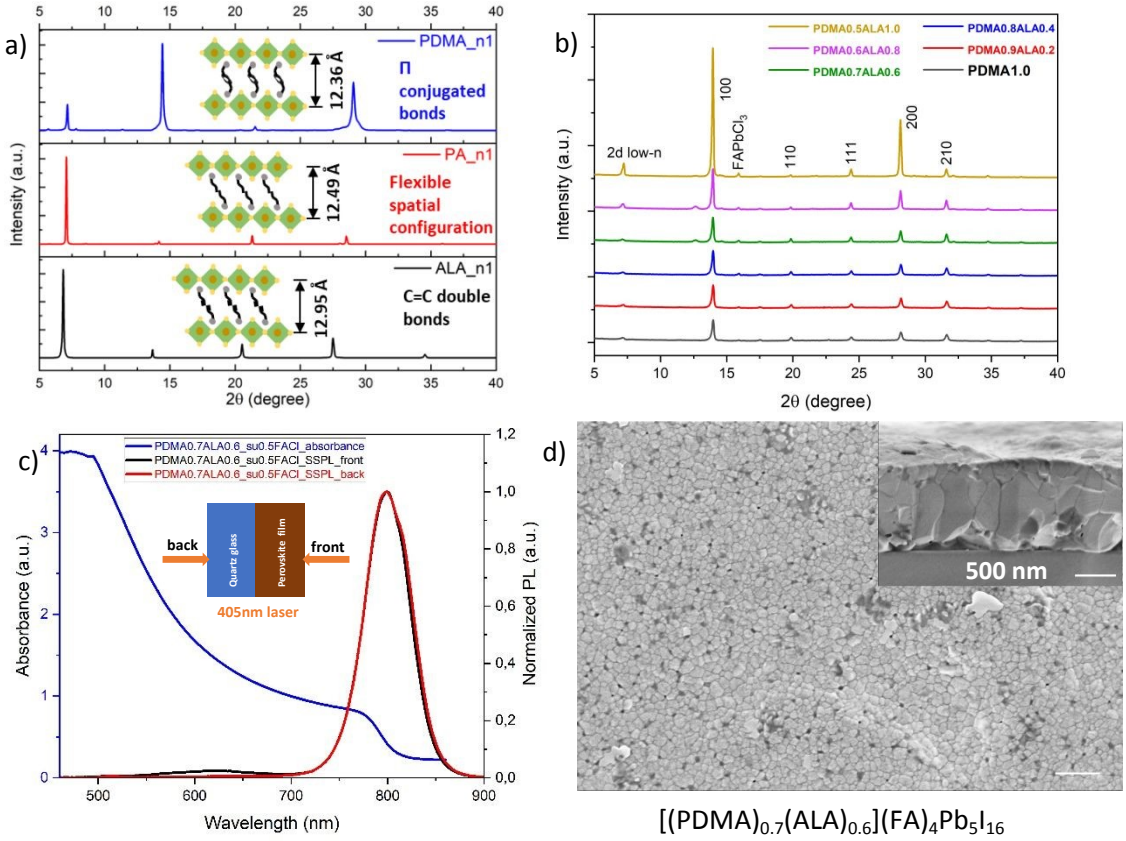

Figure 5. Crystallography, optical properties, phase distribution and surface morphology of quasi-2D perovskites with mixed PDMA and ALA spacers. (a) Powder X-ray diffractograms of pure 2D perovskites $(L)_mPbI_4$, where L = PDMA, PA, ALA, and the corresponding interlayer distances. (b) Powder X-ray diffractograms of quasi-2D perovskites $[(PDMA)_{1-x}((ALA)_2)_x](FA)_4Pb_5I_{16}$ (x = 0, 0.1, 0.2, 0.3, 0.4, 0.5) with spacers mixing. (c) UV-Vis absorption spectra and steady-state PL from front (perovskite) and back (substrate) sides of the film $[(PDMA)_{0.7}(ALA)_{0.6}](FA)_4Pb_5I_{16}$ with 50 mol% FACl substitution. (c) Surface morphology of the film $[(PDMA)_{0.7}(ALA)_{0.6}](FA)_4Pb_5I_{16}$ with 50 mol% FACl substitution. Inset is the cross-sectional view, both scale bars are 500 nm.

View Article Online
DOI: 10.1039/D4TC02231A

Open Access Article. Published on 22 2024. Downloaded on 22-08-2024 8:22:30.
This article is licensed under a Creative Commons Attribution 3.0 Unported Licence.

Journal of Materials Chemistry C Accepted Manuscript

Adopting the substitutional FACl doping strategy and substituting 50 mol% FAI for FACl, a perovskite-phase with the nominal chemical formula $[(PDMA)_{1-x}((ALA)_2)_x](FA)_4Pb_5I_{16}$ was formed. With an increasing ratio of ALA with respect to PDMA, the quasi-2D perovskites with $\langle n \rangle = 5$ all showed the stable α-phase and increasing crystallinity (**Figure 5b**). No XRD peak splitting was observed, possibly because ALA is a rigid molecule with C=C double bonds as compared to other Ruddlesden-Popper spacers with C-C single bonds such as PA, which have more degrees of freedom for spatial rearrangement and molecular relaxation. For example, the film $[(PDMA)_{0.7}(ALA)_{0.6}](FA)_4Pb_5I_{16}$ (x = 0.3) had a strong light absorption with a sharp absorption onset edge (**Figure 5c**). The steady-state PL spectra in **Figure 5c** showed a similar reversed-gradient phase distribution as the film $(PDMA)(FA)_4Pb_5I_{16}$ with substitutional FACl doping, i.e. the 2D low-*n* domains reside on the top side, and the 3D domain at the bottom side of the film. Thus, ALA spacer mixing did not change the phase distribution. It was the additive doping method and the different crystallization mechanism that determined the changed evolution of the phase distribution. It is worth noting that the dominant PL band from the back excitation had a small shoulder, implying that it can comprise of two separate emission bands very close to each other. A possible reason might be that although the 3D domain normally does not contain spacers, the octahedra in quasi-2D perovskites are locally tilted induced by the two spacers, generating two distinct PL bands. Another possible reason lies on the trap state involved reabsorption and reemission. Furthermore, ALA spacer mixing did change the surface morphology. In contrast to the pristine film $(PDMA)(FA)_4Pb_5I_{16}$, which had a rough surface (**Figure S3a**), and the film $(ALA)_2(FA)_4Pb_5I_{16}$ with crystallites (**Figure S3c**), the surface morphology of the film $[(PDMA)_{0.7}(ALA)_{0.6}](FA)_4Pb_5I_{16}$ with spacer mixing contained grains resembling the film $(PDMA)(FA)_4Pb_5I_{16}$ with substitutional FACl additive (**Figure 4c**). But the vertically aligned grains had grown even larger, spanning the whole film thickness (**Figure 5d**), which may facilitate out-of-plane charge carrier transport. The most likely reason is that the ALA spacer can fix the missing bridging to adjacent octahedra left by the bulky PDMA spacers. The better aligned interlayer connections led to an improved vertically aligned crystal growth over larger distances.[45]

2.2.4 Spacer mixing of PDMA and PA

Since the doping method controls the phase distribution, we explored spacer mixing of PDMA and PA based on the pristine film $(PDMA)(FA)_4Pb_5I_{16}$ using a DMF/NMP co-solvent system and 10 mol% excess MACl, and investigated the effect of PA mixing and A-site cation mixing on crystallization and phase distribution manipulation. 2D perovskites with a PA spacer have an interlayer distance of 12.49 Å, very similar to that of PDMA (**Figure 5a**). Following prior experience [41], we chose a stoichiometric ratio of spacers $((PDMA)_{0.7}(PA)_{0.6})$ for L-site spacer mixing. For A-site cation mixing, we first explored FA and MA mixing based on the film composition $(PA)_2[(FA)_{1-x}(MA)_x]Pb_5I_{16}$ where x = 0, 0.1, 0.3, 0.5, 0.7, 0.9, or 1, since incorporating small-sized MA can help release lattice strain induced by the larger sized FA, while maintaining thermal and structural stability. In **Figure S4a**, it can be seen that the (100) peak slightly moved to a higher angle with increasing ratio of MA, implying that the smaller-sized MA incorporated into the perovskite structure. The bandgap changed from 1.53 eV for FA-based (x = 0) to 1.61 eV for full MA-based (x = 1) quasi-2D perovskites (see Tauc plot in **Figure S4b**). This result is consistent with the steady-state PL spectra in **Figure S4c**, where the FA-based quasi-2D perovskite showed an emission band around 793 nm, and it was blue-shifted to 759 nm upon MA substitution. Thus, the bandgap can also be tuned by A-site cation mixing.

View Article Online
DOI: 10.1039/D4TC02231A

L-site spacers and A-site cations were mixed according to the chemical formula $[(PDMA)_{0.7}(PA)_{0.6}][(FA)_{1-x}(MA)_x]_4Pb_5I_{16}$ (x = 0, 0.05, 0.1, 0.15, 0.2, 0.25). Since we want FA to dominate the properties for its smaller bandgap and higher thermal stability, the A-site cation mixing ratio was kept below 25 mol% of MA. Different mixing ratios all showed a stable α-phase, but the XRD data in **Figure 6a** also showed a peak split. We assume that, although the two spacers have very similar interlayer distances, the penetration depth of the ammonium heads are slightly different, which probably induces octahedral tilting and splitting of the peak (**Figure 6b**). The d-spacings from the split peak (6.32 Å and 6.16 Å) match the nuance of the interlayer distances of the two spacers (12.49 Å and 12.36 Å, respectively).

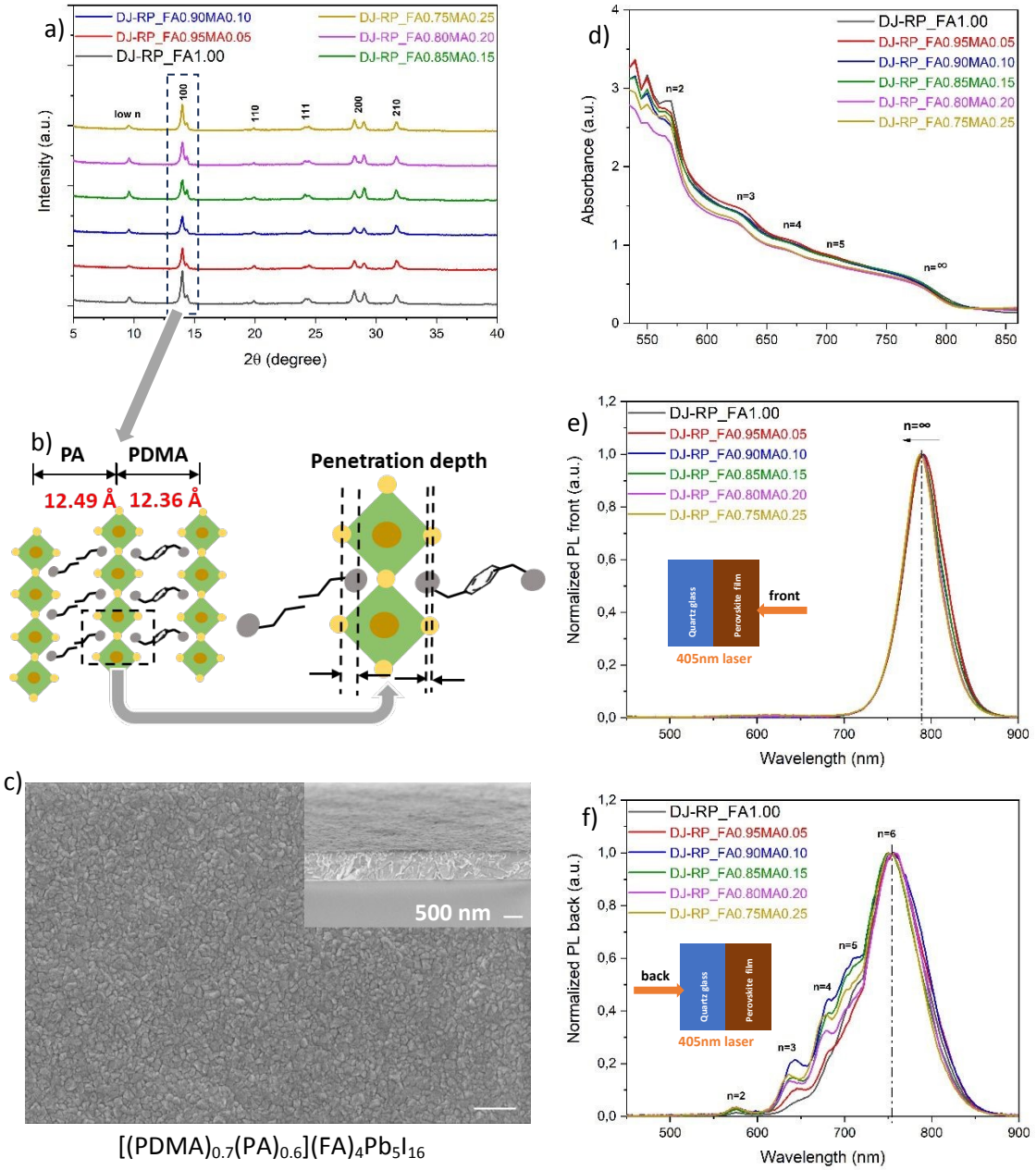

Figure 6. Crystallography, surface morphology, optical properties and phase distribution of quasi-2D perovskites with PDMA and PA spacer mixing and A-site cation mixing. In the labels, "DJ-RP" refers to the mixed system DJ spacer PDMA - RP spacer PA, and "$(FA)_{1-x}(MA)_x$" describes the A-site mixing ratio.

Open Access Article. Published on 22 2024. Downloaded on 22-08-2024 8:22:30.
This article is licensed under a Creative Commons Attribution 3.0 Unported Licence.

Journal of Materials Chemistry C Accepted Manuscript

View Article Online
DOI: 10.1039/D4TC02231A

(a) Powder X-ray diffractograms. (b) Schematic illustration of spacers mixing of PDMA and PA and the corresponding interlayer distance and penetration depth differences. (c) Surface morphology of the film $[(PDMA)_{0.7}(PA)_{0.6}](FA)_4Pb_5I_{16}$. The inset shows the cross-sectional view, both scale bars are 500 nm. (d) UV-Vis absorption spectra. (e) Steady-state PL spectrum, recorded using front (perovskite) side excitation at 405 nm. (f) Steady-state PL spectrum , recorded using back (substrate) side excitation at 405 nm.

Figure 6d shows the UV-Vis absorption spectra. In addition to the absorption onset, multiple excitonic bands were present, representing multiple microstructural domains of different *n* value in the quasi-2D perovskites. In the steady-state PL spectra from the front excitation, only one dominating emission band in average of 789 nm was observed, corresponding to the presence of 3D domain (**Figure 6e**). The band was slightly blue-shifted from 792 nm to 788 nm upon MA substitution. For the back excitation, the steady-state PL spectra in **Figure 6f** shows multiple emission bands of 2D low-*n* domains as expected and consistent with the UV-Vis absorption spectra. The results imply that the phase distribution was regulated to a normal-gradient type, compared to the pristine film $(PDMA)(FA)_4Pb_5I_{16}$ and its random phase distribution in **Figure 2b**. A novel discovery was that the maximum emission at the bottom side of film occurred around 754 nm. We assume that this belongs to an even higher *n*-valued domain, probably *n* = 6. Layered perovskite with n ≥ 6-7 domains have been proposed to be thermodynamically unfavourable or unstable [60], but the *n* = 6 domain may have formed because the spacer mixing of PDMA and PA favoured the thermodynamics and lowered the formation energy of higher *n*-valued domains. With 3D domains on the top side and 2D low-*n* domains at the bottom side, this normal-gradient phase distribution with regulated quantum-well structure can facilitate a preferential energy transfer cascade. Taking the film $[(PDMA)_{0.7}(PA)_{0.6}](FA)_4Pb_5I_{16}$ as an example, the surface morphology in **Figure 6c** showed fine grains and relatively smooth surface compared to either $(PDMA)(FA)_4Pb_5I_{16}$ or $(PA)_2(FA)_4Pb_5I_{16}$ film without spacers mixing (**Figure S3a and S3b**), implying that a lower number of defects and improved interfacial contact with another charge transport layer on top were generated by this spacer mixing method.

Film growth and phase distribution regulation via the different manipulation strategies are showcased in **Figure 7**. With excessive FACl additive doping, the *n* = 2 domain is eventually formed on the top surface of the film, especially at the grain boundaries (**Figure 7a**). With substitutional FACl doping, the 2D low-*n* domains (*n* = 1, 3) are formed mainly at the top of the film, embedded in the 3D domain matrix, yielding a revered-gradient (**Figure 7b**), whether using only PDMA spacer or using mixed spacers PDMA and ALA. Finally, when using the mixed spacers PDMA and PA, the 2D domains (*n* = 2-6) are formed mainly at the bottom of the film, yielding a normal-gradient (**Figure 7c**). All crystallization engineering strategies can regulate the phase distribution of quasi-2D perovskites compared to the pristine film.

Open Access Article. Published on 22 2024. Downloaded on 22-08-2024 8:22:30.
This article is licensed under a Creative Commons Attribution 3.0 Unported Licence.

Journal of Materials Chemistry C Accepted Manuscript

View Article Online
DOI: 10.1039/D4TC02231A

Open Access Article. Published on 22 2024. Downloaded on 22-08-2024 8:22:30.
This article is licensed under a Creative Commons Attribution 3.0 Unported Licence.

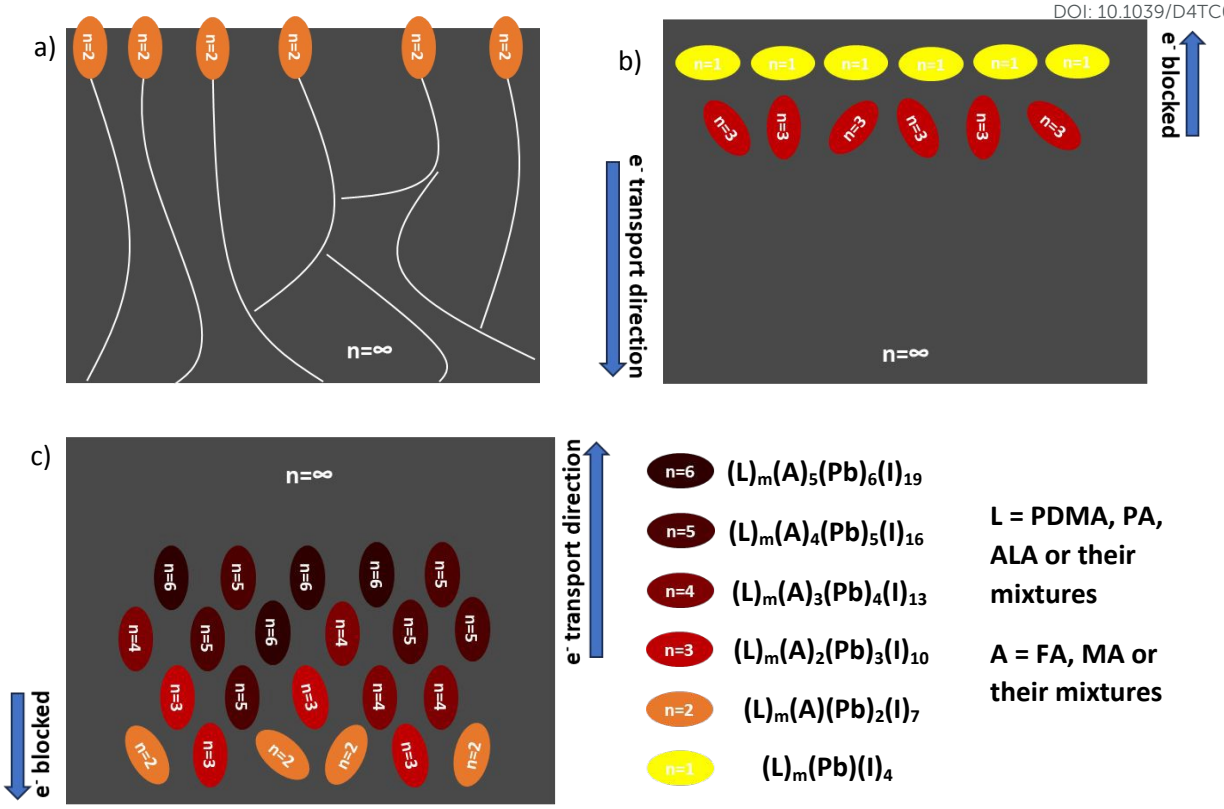

Figure 7. Schematic illustration of the film growth in cross-sectional view and the regulated phase distributions following different manipulation strategies. (a) 2D low-*n* crystals at the top surface and at the grain boundaries of 3D domains in (PDMA)$(FA)_4Pb_5I_{16}$ film with excess FACl doping. (b) Reversed-gradient phase distribution of (PDMA)$(FA)_4Pb_5I_{16}$ film and $[(PDMA)_{1-x}((ALA)_2)_x](FA)_4Pb_5I_{16}$ film with FACl substitutional doping. (c) Normal-gradient phase distribution of $[(PDMA)_{0.7}((PA)_2)_{0.3}][(FA)_{1-x}(MA)_x]_4Pb_5I_{16}$ film with 10 mol% excess MACl doping.

3. Conclusions

Different manipulation strategies were implemented to regulate the phase distribution of Dion-Jacobson-type quasi-2D perovskites based on the composition of $(PDMA)FA_4Pb_5I_{16}$. In general, FACl additive doping changed the crystallization kinetics, leading to 2D low-*n* crystals on the top surface or a reversed-gradient phase distribution, following either an excess doping or a substitutional doping method. Alternatively, mixing with another Ruddlesden-Popper spacer fixed the missing bridging to the adjacent octahedra, regulating the quantum-well structures into a normal-gradient phase distribution. Combining both FACl doping and spacer mixing, the film showed properties from both manipulation strategies, i.e. a reversed-gradient phase distribution and larger vertically aligned grains.

4. Experimental Section

Materials: Lead (II) iodide (PbI_2, 99.999%), Methylammonium iodide (MAI, ⩾99%), Formamidinium iodide (FAI, ⩾99%) N,N-Dimethylformamide (DMF, 99.8%), Dimethyl sulfoxide (DMSO, ⩾99.9%), p-Xylylenediamine (PDMA, 99%), Allylamine (ALA, 98%), Hydroiodic acid 57% (HI, for synthesis), Diethyl

Journal of Materials Chemistry C Accepted Manuscript

View Article Online
DOI: 10.1039/D4TC02231A

ether (⩾99.9%) were purchased from Sigma-Aldrich. Propylamine (PA, ⩾99.0%) was purchased from Fluka. The abovementioned chemicals were used as received without further purification. Methylammonium chloride (MACl, for synthesis) was purchased from Sigma-Aldrich, and was further dried in a vacuum oven before use.

Synthesis of $PDMAI_2$ powder: First 3.485 g PDMA was dissolved in ethanol with stirring. Then 7.37 ml HI was added, and heated at 100°C in an oil bath, until all precipitates were solidified and all liquid was evaporated. The yellowish clay-like precipitates were purified with diethyl ether, followed by transferring them into a petri-dish. Finally, the precipitates were dried in a 60°C vacuum oven for 3 days.

Synthesis of PAI powder: First 13.20 ml HI was added into 8.29 ml PA, and then heated at 100°C in an oil bath with continuous stirring, until all precipitates were solidified and all liquid was evaporated. The precipitates were purified with a large amount of diethyl ether until they turned white. This step was followed by transferring them into a petri-dish. Finally, the precipitates were dried in a 60°C vacuum oven for 3 days.

Synthesis of ALAI powder: First 12.30 ml cold HI was added dropwise into 7.50 ml ALA dissolved in 20 ml IPA in an ice bath and gradually brought back to room temperature. Then the mixture was heated at 70°C until the precipitates were solidified and all liquid was evaporated. The precipitates were purified with a large amount of diethyl ether until they turned beige. The precipitates were dried on a 60°C hotplate for 30 min.

Preparation of precursor solutions: For the <*n*>=5 Dion-Jacobson precursor solution, $PDMAI_2$, FAI and PbI_2 powders were dissolved in a stoichiometric molar ratio of 1:4:5 with a Pb^{2+} concentration of 1M in the mixed solvent DMF:NMP=9:1. Doping with excess FACl was done by increasing the molar FACl:PbI_2 ratio to a higher value than 4:5 while keeping Pb^{2+} in the precursor solution constant. For compensated FACl additive doping, FAI was substituted by FACl in the ratio of FAI:FACl = (1-*x*):*x*. For <*n*>=5 mixed Dion-Jacobson and Ruddlesden-Popper spacers and mixed A-site cations precursor solution, $PDMAI_2$, PAI or ALAI, FAI, MAI and PbI_2 powders were dissolved in the stoichiometric molar ratio (1-*x*):2*x*:4(1-*y*):4*y*:5.

Fabrication of quasi-2D perovskite thin films: First the ultra-flat quartz-coated glass substrate was sequentially cleaned with detergent, DI water, acetone and IPA in an ultrasonic bath. Then the substrate was treated by O_2 plasma. After that, the substrate was transferred to the N_2 glovebox and attached to the chuck of the spin-coater, 60 µL precursor solution was dynamically spin-coated on the substrate with a stepwise spinning program of 1500 rpm for 15 s and 4000 rpm for 20 s. During the second step, 180 µL chlorobenzene was dripped quickly onto the substrate. The final film was formed by post-annealing at 150°C on a hotplate for 10 min.

Characterization: Powder x-ray diffraction (XRD) was done by a Panalytical X'pert Pro Powder diffractometer with Cu $K\alpha_1$ radiation. The UV-Vis absorption spectra were measured using a UV/VIS/NIR Perkin Elmer Lambda 950 Spectrometer in transmittance (T) mode, after which the absorbance (A) was calculated from A = 2 – log *T*. Steady-state photoluminescence was measured by a Blue-Wave Spectrometer from StellarNet Inc with a 405 nm laser from MatchBox series and a FGL435S color filter from Thorlabs. Scanning electron microscopy (SEM) (point resolution) was measured with a Zeiss Merlin HR-SEM equipped with energy dispersive x-ray spectroscopy (EDX) (spatial resolution).

Open Access Article. Published on 22 2024. Downloaded on 22-08-2024 8:22:30.
This article is licensed under a Creative Commons Attribution 3.0 Unported Licence.

Journal of Materials Chemistry C Accepted Manuscript

View Article Online
DOI: 10.1039/D4TC02231A

Open Access Article. Published on 22 2024. Downloaded on 22-08-2024 8:22:30.
This article is licensed under a Creative Commons Attribution 3.0 Unported Licence.

Journal of Materials Chemistry C Accepted Manuscript

Author Information

Corresponding author:

Johan E. ten Elshof (j.e.tenelshof@utwente.nl, orcid.org/0000-0001-7995-6571)

Authors:

Xiao Zhang (x.zhang-6@utwente.nl, orcid.org/0009-0007-1448-3225)

Lisanne Einhaus (l.m.einhaus@utwente.nl, orcid.org/0009-0003-8908-5126)

Annemarie Huijser (j.m.huijser@utwente.nl, orcid.org/0000-0003-0381-6155)

Author Contributions

The manuscript was written through contributions of all authors. All authors have given approval to the final version of the manuscript.

Conflict of Interest

The authors declare no conflict of interest.

Acknowledgements

Financial support of project TTW 17711 from the Dutch Research Council (NWO) Domain Applied and Engineering Sciences is gratefully acknowledged.

Keywords

Quasi-2D perovskite, formamidinium, phase distribution, solution engineering, additive doping, spacer mixing

References

1. I. C. Smith, E. T. Hoke, D. Solis-Ibarra, M. D. McGehee and H. I. Karunadasa, *Angew Chem Int Ed Engl*, 2014, **53**, 11232-11235.
2. Y. Yang, F. Gao, S. Gao and S.-H. Wei, *Journal of Materials Chemistry A*, 2018, **6**, 14949-14955.
3. Z. Huang, A. H. Proppe, H. Tan, M. I. Saidaminov, F. Tan, A. Mei, C.-S. Tan, M. Wei, Y. Hou, H. Han, S. O. Kelley and E. H. Sargent, *ACS Energy Letters*, 2019, **4**, 1521-1527.
4. C. Liang, D. Zhao, Y. Li, X. Li, S. Peng, G. Shao and G. Xing, *Energy & Environmental Materials*, 2018, **1**, 221-231.
5. Y. Liu, H. Zhou, Y. Ni, J. Guo, R. Lu, C. Li and X. Guo, *Joule*, 2023, **7**, 1016-1032.
6. D. Thrithamarassery Gangadharan and D. Ma, *Energy & Environmental Science*, 2019, **12**, 2860-2889.

View Article Online
DOI: 10.1039/D4TC02231A

Open Access Article. Published on 22 2024. Downloaded on 22-08-2024 8:22:30.
This article is licensed under a Creative Commons Attribution 3.0 Unported Licence.

7. I. Spanopoulos, I. Hadar, W. Ke, Q. Tu, M. Chen, H. Tsai, Y. He, G. Shekhawat, V. P. Dravid, M. R. Wasielewski, A. D. Mohite, C. C. Stoumpos and M. G. Kanatzidis, *J Am Chem Soc*, 2019, **141**, 5518-5534.
8. B. R. Wygant, A. Z. Ye, A. Dolocan, Q. Vu, D. M. Abbot and C. B. Mullins, *J Am Chem Soc*, 2019, **141**, 18170-18181.
9. T. L. Leung, I. Ahmad, A. A. Syed, A. M. C. Ng, J. Popović and A. B. Djurišić, *Communications materials*, 2022, **3**, 63.
10. H. Zheng, G. Liu, L. Zhu, J. Ye, X. Zhang, A. Alsaedi, T. Hayat, X. Pan and S. Dai, *Advanced Energy Materials*, 2018, **8**, 1800051.
11. S. Yang, Y. Wang, P. Liu, Y.-B. Cheng, H. J. Zhao and H. G. Yang, *Nature Energy*, 2016, **1**, 1-7.
12. M. Shao, T. Bie, L. Yang, Y. Gao, X. Jin, F. He, N. Zheng, Y. Yu and X. Zhang, *Adv Mater*, 2022, **34**, e2107211.
13. V. M. Goldschmidt, *Naturwissenschaften*, 1926, **14**, 477-485.
14. F. Zhang, H. Lu, J. Tong, J. J. Berry, M. C. Beard and K. Zhu, *Energy & Environmental Science*, 2020, **13**, 1154-1186.
15. C. Ortiz-Cervantes, P. Carmona-Monroy and D. Solis-Ibarra, *ChemSusChem*, 2019, **12**, 1560-1575.
16. C. C. Stoumpos, D. H. Cao, D. J. Clark, J. Young, J. M. Rondinelli, J. I. Jang, J. T. Hupp and M. G. Kanatzidis, *Chemistry of Materials*, 2016, **28**, 2852-2867.
17. C. C. Stoumpos, C. M. M. Soe, H. Tsai, W. Nie, J.-C. Blancon, D. H. Cao, F. Liu, B. Traoré, C. Katan, J. Even, A. D. Mohite and M. G. Kanatzidis, *Chem*, 2017, **2**, 427-440.
18. L. Mao, W. Ke, L. Pedesseau, Y. Wu, C. Katan, J. Even, M. R. Wasielewski, C. C. Stoumpos and M. G. Kanatzidis, *J Am Chem Soc*, 2018, **140**, 3775-3783.
19. X. Li, W. Ke, B. Traore, P. Guo, I. Hadar, M. Kepenekian, J. Even, C. Katan, C. C. Stoumpos, R. D. Schaller and M. G. Kanatzidis, *J Am Chem Soc*, 2019, **141**, 12880-12890.
20. G. Wu, R. Liang, Z. Zhang, M. Ge, G. Xing and G. Sun, *Small*, 2021, **17**, e2103514.
21. W. Paritmongkol, N. S. Dahod, A. Stollmann, N. Mao, C. Settens, S.-L. Zheng and W. A. Tisdale, *Chemistry of Materials*, 2019, **31**, 5592-5607.
22. C. Fu, Z. Gu, Y. Tang, Q. Xiao, S. Zhang, Y. Zhang and Y. Song, *Angew Chem Int Ed Engl*, 2022, **61**, e202117067.
23. Z. Xing, X. Meng, D. Li, Y. Zhang, B. Fan, Z. Huang, F. Wang, X. Hu, T. Hu and Y. Chen, *Angew Chem Int Ed Engl*, 2023, **62**, e202303177.
24. L. Pedesseau, D. Sapori, B. Traore, R. Robles, H. H. Fang, M. A. Loi, H. Tsai, W. Nie, J. C. Blancon, A. Neukirch, S. Tretiak, A. D. Mohite, C. Katan, J. Even and M. Kepenekian, *ACS Nano*, 2016, **10**, 9776-9786.
25. C. C. Stoumpos and M. G. Kanatzidis, *Adv Mater*, 2016, **28**, 5778-5793.
26. Y. Wei, B. Chen, F. Zhang, Y. Tian, X. Yang, B. Cai and J. Zhao, *Solar RRL*, 2021, **5**, 2000661.
27. S. Masi, A. F. Gualdrón-Reyes and I. Mora-Seró, *ACS Energy Letters*, 2020, **5**, 1974-1985.
28. Y. Huang, X. Lei, T. He, Y. Jiang and M. Yuan, *Advanced Energy Materials*, 2022, **12**, 2100690.
29. K. Li and H. Zhou, *Chinese Journal of Chemistry*, 2023, **41**, 2730-2745.
30. Y. Zhang, S. G. Kim, D. K. Lee and N. G. Park, *ChemSusChem*, 2018, **11**, 1813-1823.
31. G. Li, Z. Wang, Y. Wang, Z. Yang, P. Dong, Y. Feng, Y. Jiang, S. P. Feng, G. Zhou, J. M. Liu and J. Gao, *Small*, 2023, **19**, e2301323.
32. L. Cheng, Z. Liu, S. Li, Y. Zhai, X. Wang, Z. Qiao, Q. Xu, K. Meng, Z. Zhu and G. Chen, *Angew Chem Int Ed Engl*, 2021, **60**, 856-864.
33. G. Wu, T. Liu, M. Hu, Z. Zhang, S. Li, L. Xiao, J. Guo, Y. Wang, A. Zhu, W. Li, H. Zhou, Y. Zhang, R. Chen and G. Xing, *Adv Mater*, 2023, **35**, e2303061.
34. T. Bu, J. Li, H. Li, C. Tian, J. Su, G. Tong, L. K. Ono, C. Wang, Z. Lin and N. Chai, *Science*, 2021, **372**, 1327-1332.
35. X. Du, J. Zhang, H. Su, X. Guo, Y. Hu, D. Liu, N. Yuan, J. Ding, L. Gao and S. F. Liu, *Adv Mater*, 2022, **34**, e2204098.

Journal of Materials Chemistry C Accepted Manuscript

View Article Online
DOI: 10.1039/D4TC02231A

36. T. Bu, L. K. Ono, J. Li, J. Su, G. Tong, W. Zhang, Y. Liu, J. Zhang, J. Chang, S. Kazaoui, F. Huang, Y.-B. Cheng and Y. Qi, *Nature Energy*, 2022, **7**, 528-536.
37. J. Yan, W. Qiu, G. Wu, P. Heremans and H. Chen, *Journal of Materials Chemistry A*, 2018, **6**, 11063-11077.
38. N. Liu, P. Liu, H. Ren, H. Xie, N. Zhou, Y. Gao, Y. Li, H. Zhou, Y. Bai and Q. Chen, *ACS Appl Mater Interfaces*, 2020, **12**, 3127-3133.
39. L. Min, W. Tian, F. Cao, J. Guo and L. Li, *Adv Mater*, 2021, **33**, e2101714.
40. Z. Xu, D. Lu, F. Liu, H. Lai, X. Wan, X. Zhang, Y. Liu and Y. Chen, *ACS Nano*, 2020, **14**, 4871-4881.
41. G. Wu, X. Li, J. Zhou, J. Zhang, X. Zhang, X. Leng, P. Wang, M. Chen, D. Zhang, K. Zhao, S. F. Liu, H. Zhou and Y. Zhang, *Adv Mater*, 2019, **31**, e1903889.
42. S. Peng, J. Ma, P. Li, S. Zang, Y. Zhang and Y. Song, *Advanced Functional Materials*, 2022, **32**, 2205289.
43. Y. Yang, C. Liu, H. Kanda, Y. Ding, H. Huang, H. Chen, B. Ding, Y. Liang, X. Liu and M. Cai, *Advanced Functional Materials*, 2021, **31**, 2104868.
44. W. Li, X. Feng, K. Guo, W. Pan, M. Li, L. Liu, J. Song, Y. He and H. Wei, *Adv Mater*, 2023, **35**, e2211808.
45. X. Zhang, L. Einhaus, A. Huijser and J. E. Ten Elshof, *Inorg Chem*, 2024, **63**, 5246-5259.
46. D. Yu, F. Cao, C. Su and G. Xing, *Acc Chem Res*, 2023, **56**, 959-970.
47. G. Ren, Z. Zhang, Y. Deng, Z. Li, C. Liu, M. Wang and W. Guo, *Energy & Environmental Science*, 2023, **16**, 565-573.
48. Y. Ma, C. Zeng, P. Zeng, Y. Hu, F. Li, Z. Zheng, M. Qin, X. Lu and M. Liu, *Adv Sci (Weinh)*, 2023, **10**, e2205072.
49. R. Azmi, E. Ugur, A. Seitkhan, F. Aljamaan, A. S. Subbiah, J. Liu, G. T. Harrison, M. I. Nugraha, M. K. Eswaran and M. Babics, *Science*, 2022, **376**, 73-77.
50. Yukta, N. Parikh, R. D. Chavan, P. Yadav, M. K. Nazeeruddin and S. Satapathi, *ACS Appl Mater Interfaces*, 2022, **14**, 29744-29753.
51. X. Jiang, J. Zhang, S. Ahmad, D. Tu, X. Liu, G. Jia, X. Guo and C. Li, *Nano Energy*, 2020, **75**, 104892.
52. Y. Yu, R. Liu, M. Xu and H. Yu, *EcoMat*, 2023, **5**, e12272.
53. G. Wu, R. Liang, M. Ge, G. Sun, Y. Zhang and G. Xing, *Adv Mater*, 2022, **34**, e2105635.
54. M. Degani, Q. An, M. Albaladejo-Siguan, Y. J. Hofstetter, C. Cho, F. Paulus, G. Grancini and Y. Vaynzof, *Science advances*, 2021, **7**, eabj7930.
55. Y. Liu, J. Guo, H. Zhou, C. Li and X. Guo, *J Am Chem Soc*, 2024, **146**, 8198-8205.
56. S. Yu, Y. Yan, M. Abdellah, T. Pullerits, K. Zheng and Z. Liang, *Small*, 2019, **15**, e1905081.
57. A. H. Proppe, M. Wei, B. Chen, R. Quintero-Bermudez, S. O. Kelley and E. H. Sargent, *J Am Chem Soc*, 2019, **141**, 14180-14189.
58. S. Yu, M. Abdellah, T. Pullerits, K. Zheng and Z. Liang, *Advanced Functional Materials*, 2021, **31**, 2104342.
59. N. Zhou, B. Huang, M. Sun, Y. Zhang, L. Li, Y. Lun, X. Wang, J. Hong, Q. Chen and H. Zhou, *Advanced Energy Materials*, 2020, **10**, 1901566.
60. C. M. M. Soe, G. P. Nagabhushana, R. Shivaramaiah, H. Tsai, W. Nie, J. C. Blancon, F. Melkonyan, D. H. Cao, B. Traore, L. Pedesseau, M. Kepenekian, C. Katan, J. Even, T. J. Marks, A. Navrotsky, A. D. Mohite, C. C. Stoumpos and M. G. Kanatzidis, *Proc Natl Acad Sci U S A*, 2019, **116**, 58-66.

Open Access Article. Published on 22 2024. Downloaded on 22-08-2024 8:22:30.
This article is licensed under a Creative Commons Attribution 3.0 Unported Licence.

Journal of Materials Chemistry C Accepted Manuscript

View Article Online
DOI: 10.1039/D4TC02231A

The data supporting this article have been included as part of the Supplementary Information.

Open Access Article. Published on 22 2024. Downloaded on 22-08-2024 8:22:30.
This article is licensed under a Creative Commons Attribution 3.0 Unported Licence.

Journal of Materials Chemistry C Accepted Manuscript